Global Change Biology

WILEY

Global Change Biology

RESEARCH ARTICLE OPEN ACCESS

Resilience Indicators for Tropical Rainforests in a Dynamic Vegetation Model

Sebastian Bathiany[1,2] | Da Nian[1,2] | Markus Drüke[2,3] | Niklas Boers[1,2,4]

[1]Earth System Modelling, School of Engineering and Design, Technical University of Munich, Munich, Germany | [2]Potsdam Institute for Climate Impact Research, Potsdam, Germany | [3]Deutscher Wetterdienst, Hydrometeorologie, Offenbach, Germany | [4]Department of Mathematics and Global Systems Institute, University of Exeter, Exeter, UK

Correspondence: Sebastian Bathiany (sebastian.bathiany@tum.de)

Received: 24 February 2024 | **Revised:** 15 October 2024 | **Accepted:** 18 November 2024

Funding: This is ClimTip contribution #3; the ClimTip project has received funding from the European Union's Horizon Europe research and innovation programme under grant agreement No. 101137601.

Keywords: Amazon rainforest | climate change | critical slowing down | dynamic global vegetation models | early warning signals | ecosystem resilience | tipping points

ABSTRACT

Tropical forests and particularly the Amazon rainforest have been identified as potential tipping elements in the Earth system. According to a dynamical systems theory, a decline in forest resilience preceding a potential shift to a savanna-like biome could manifest as increasing autocorrelation of biomass time series. Recent satellite records indeed exhibit such a trend and also show larger autocorrelation, indicative of reduced resilience, in drier forest regions. However, it is unclear which processes underlie these observational findings and on which scales they operate. Here, we investigate which processes determine tropical forest resilience in the stand-alone, state-of-the-art dynamic global vegetation model LPJmL. We find that autocorrelation is higher in dry climates than wet climates (approx. 0.75 vs. 0.2, for a lag of 10 years), which qualitatively agrees with observations. By constructing a reduced version of LPJmL and by disabling and enabling certain processes in the model, we show that (i) this pattern is associated with population dynamics operating on different time scales in different climates and (ii) that the pattern is sensitive to the allocation of carbon to different pools, especially in years of stress. Both processes are highly uncertain, oversimplified or even lacking in most Earth system models. Our results indicate that the observed spatial variations and trends in vegetation resilience indicators may be explained by local physiological and ecological mechanisms alone, without climate–vegetation feedbacks. In principle, this is consistent with the view that the Amazon rainforest is responding to climate change locally and does not necessarily need to approach one large-scale tipping point, although the latter cannot be ruled out based on our findings.

1 | Introduction

Tropical forests, and the Amazon rainforest in particular, are among the components of the climate system that have been identified as potential "tipping elements" (Lenton et al. 2008). This assessment reflects the concern that as global warming and tropical deforestation are progressing, the nonlinearities in a rainforest's response to warming, which involves positive atmosphere-vegetation feedbacks, can lead to comparably abrupt large-scale loss of forest cover, carbon pools, and biodiversity (Cox et al. 2004; Malhi et al. 2009; Nobre and Borma 2009; Lovejoy and Nobre 2019). On a mathematical level, dynamical systems theory describes how a nonlinear system that exhibits positive feedbacks can become increasingly sensitive to small gradual changes in forcing. In the extreme case, this can lead to the existence of a bifurcation point, where a stable state is suddenly lost (Scheffer et al. 2001). For any given forcing, the stability of the stable state can be

measured as the system's recovery rate to equilibrium after being perturbed (Wissel 1984). While large perturbations are rare in practice, one can also diagnose resilience using indicators like variance and autocorrelation from the natural variability without directly interfering in the system (Kleinen, Held, and Petschel-Held 2003; Held and Kleinen 2004; Scheffer et al. 2009; Boers, Ghil, and Stocker 2022). During the process of destabilization, the recovery rate to equilibrium decreases, a phenomenon called "critical slowing down" (CSD), which then leads to increasing variance and autocorrelation over time. As these trends can also be observed in the situation when the system approaches a catastrophic bifurcation ("tipping point"), they have been referred to as "early warning signals" (Scheffer et al. 2009).

Recent studies have investigated "early warning signals" in observed properties of forests and other ecosystems on the globe (Smith, Traxl, and Boers 2022; Boulton, Lenton, and Boers 2022; Forzieri et al. 2022; Smith and Boers 2023b), mainly using vegetation indices computed from satellite records, like the Normalized Difference Vegetation Index (NDVI). For example, rising CSD indicators have been observed in NDVI data preceding tree mortality events in boreal North America (Rogers et al. 2018) and Californian forests (Liu et al. 2019). Wu, Vargas, et al. (2022) found increased autocorrelation in Enhanced Vegetation Index (EVI) from Landsat data during periods of ENSO-induced drought with high tree mortality in Costa Rican tropical dry forests. Hishe et al. (2021) found that sites with high precipitation and high biodiversity exhibit lower autocorrelation in the NDVI of tropical forests in Ethiopia. Satellite data also provides empirical estimates of the recovery rate after large negative perturbations induced by droughts or fires. Smith, Traxl, and Boers (2022) showed that the expected theoretical relationships between that empirical recovery rate and the statistical indicators of CSD in principle hold for vegetation dynamics as measured by vegetation optical depth (VOD).

Interestingly, statistical warning signs of tree mortality have also been observed in the radial growth rate of individual trees, though limited to particular indicators and tree species (Camarero et al. 2015; Cailleret et al. 2019). Poorter et al. (2016) used observed recovery rates of 1500 biomass records after clearing events in Latin America and found a faster recovery under wet conditions. In line with this, Smith and Boers (2023a) demonstrated that for each type of land cover, autocorrelation decreases with larger water availability on a global scale, and Verbesselt et al. (2016) analyzed NDVI and VOD in tropical forests, showing that wetter regions show smaller autocorrelation, interpreted as higher resilience. It has also been found that drought frequency and duration have an effect on CSD indicators, which indicates that not only is resilience shaped by the background climate, but individual events can also have long-lasting legacy effects on the system (Wu, Manzoni, et al. 2022; van Passel et al. 2024). Recently, Boulton, Lenton, and Boers (2022) showed that autocorrelation of VOD has been increasing in large parts of the Amazon during the last two decades, and that the resulting resilience decline is stronger in drier regions as well as in grid cells closer to human activity. Figure S1 shows a selection of results from the latter two studies. These findings support the hypothesis that a drying Amazon, as projected by climate models (Baker et al. 2021), would indeed become less resilient, that is, more vulnerable to disturbances, and might even be approaching a large-scale "tipping point."

However, observational and especially satellite records are typically very short compared to the time scale of biomass turnover and vegetation dynamics in forests (Friend et al. 2014; Cole, Bhagwat, and Willis 2014). Moreover, vegetation resilience estimates derived from satellite data can be affected by missing data and artifacts of the measurement process and post-processing, such as merging signals from multiple sensors (Smith et al. 2023). In particular, estimates of biomass and its dynamics over time are highly uncertain. Also, it is unclear which mechanisms are behind the resilience trends found in satellite records and on which time and spatial scales they operate. Conceptually, one may distinguish two idealized scenarios:

1. The detected signals reflect "early warnings" in individual trees (e.g., Camarero et al. 2015; Cailleret et al. 2019) or tree communities, which would imply a spatially heterogeneous and hence gradual forest loss as the most plausible scenario.
2. The entire ecosystem as a whole is destabilizing, involving positive atmosphere–vegetation feedbacks, which would support the view of the Amazon as a "tipping element." This scenario is supported by large-scale consistent warning signs not only in biomass (Boulton, Lenton, and Boers 2022), but specifically in precipitation (Bochow and Boers 2023).

Improved process understanding would help distinguish these scenarios and would be crucial to understand if—and under which conditions—observation-inferred CSD indicators are indeed representative for resilience changes. A better understanding would also be important to answer the question whether the observed spatial differences in CSD-based resilience estimates between wet and dry forests can be used to project the rainforest's response to a drying climate; in other words, whether "space-for-time" replacements would be justified.

To gain such understanding, and to bridge the gap between the highly complex real world and the simple concepts of dynamical systems theory and CSD, dynamic global vegetation models (DGVMs) can provide insight. Although concern over an Amazon dieback scenario dates back to model simulations using the offline "gap model" Hybrid v4.1 (White, Cannell, and Friend 1999) and the coupled climate-vegetation model HadCM3 (Cox et al. 2004), DGVMs have rarely been used for this purpose. Current simulations project a tendency of Amazon drying by coupled complex climate models used in the most recent phase of the Coupled Model Intercomparison Project, CMIP6, with some local abrupt reductions in vegetation carbon in some of the models, but no large-scale forest loss (Baker et al. 2021; Parry, Ritchie, and Cox 2022).

In general, vegetation models like the Lund-Potsdam-Jena managed Land model (LPJmL) show a nonlinear decline in carbon

pools and vegetation composition when the tropical climate changes toward drier conditions (Poulter et al. 2010; Cowling and Shin 2006; Nian et al. 2024).

The presence and reliability of CSD indicators in such simulations have remained inconclusive so far. Boulton, Good, and Lenton (2013) found increased variance in carbon pools, net primary productivity (NPP), and broadleaf fraction in a perturbed-parameter ensemble of HadCM3 with historical forcing followed by A1B projections, but no clear trends in autocorrelation. Parry, Ritchie, and Cox (2022) found in CMIP6 models that the probability of abrupt shifts increases for grid points with higher sensitivity to global warming. Applying LPJmL, Nian et al. (2024) found that a significant number of grid cells show increased autocorrelation and variance when approaching a threshold in the relationship between aboveground biomass and precipitation. The mechanisms that can generate such trends in CSD-based resilience indicators in DGVMs have not been investigated so far.

In this study, we investigate the occurrence of CSD-based resilience indicators in the terrestrial vegetation model LPJmL. Our aim is to reveal the underlying mechanisms that shape the dependency of variance and autocorrelation on precipitation in the model. Specifically, we inquire why LPJmL shows low resilience in dry climates and high resilience in wet climates. We largely focus on autocorrelation as an indicator because it is the CSD indicator most widely used in previous studies, and because our experiment design with stationary uncorrelated input assures that it is equivalent to more sophisticated CSD indicators (Boers 2021; Boettner and Boers 2022; Smith and Boers 2023b; Morr and Boers 2024). Ultimately, our aim is to better understand the observed autocorrelation patterns, though relevant processes can differ between models and observations. By revealing the relevant processes in the model, and assessing their realism, we hence also aim to derive suggestions about which processes should be improved in models and/or observed more closely in reality. Furthermore, we are motivated by the question whether climate affects vegetation resilience even without any land–atmosphere feedbacks or fire–vegetation feedbacks (i.e., for purely physiological and ecological reasons). We therefore focus on idealized "offline" simulations driven by prescribed climate.

2 | Materials and Methods

2.1 | LPJmL Model and Experiment Setup

The LPJmL (version 5) is an extensively validated and well-established process-based DGVM (Schaphoff, von Bloh, et al. 2018). While essentially being an area-averaged model (like most vegetation models in CMIP6 Earth System models), LPJmL also represents the population dynamics of trees. The input variables are 2 m temperature, precipitation, downwelling longwave radiation and downwelling shortwave radiation. As climate input, we use bias-corrected reanalysis data from the period 1979–2018 (see Section S2). Atmospheric CO_2 is held constant at 400 ppm in our simulations. We apply the model in its simplest form, without any land use or land management, wildfires, or nitrogen limitation. The default model distinguishes 11 plant functional types (PFTs): two tropical broadleaved tree types (evergreen and raingreen), three temperate tree types, three boreal tree types, tropical C4 grass, temperate C3 grass, and polar C3 grass.

In order to remove any autocorrelation in the atmospheric forcing data (and prevent that it affects the autocorrelation in the model output that we intend to analyze) and to allow for stationary simulations that are much longer than the observed record, we randomize the input data as follows: At each grid cell, for every simulation day, we prescribe atmospheric conditions from the correct calendar day of the year but from a randomly chosen year in the climate input data (using a 365-day calendar without leap days). This method allows us to keep the observed annual cycle and correlations between variables while removing autocorrelation from day to day.

Our study involves simulations with the full LPJmL model as well as a number of reduced and/or modified versions (see Table 1). We first perform a geographically explicit simulation for the domain of Meso and South America (EXP1), where the climate input data is unmodified apart from the shuffling procedure explained above. Second, in order to systematically explore the sensitivity of vegetation to environmental conditions without having to simulate too many grid cells, we also construct an idealized tropical rainforest domain of 20×20 grid cells (EXP2 and EXP3). In this domain, the annual mean and the seasonality of precipitation show linear gradients in the longitudinal and latitudinal direction, respectively. Here, all atmospheric forcing is taken from a rectangular box located in the central Amazon basin (70 W–66.5 W, 3.25 S–0°, corresponding to 7×7 grid cells). We posit that our results are still valid for tropical rainforests in general because even in realistic domains, the same vegetation model is applied pointwise at each grid cell individually. In contrast to the spatially explicit experiment EXP1, the input randomization here involves picking not only a random year, but also a random grid cell from the 7×7 observational domain, for each individual simulation day and grid cell. This procedure results in a slight variance increase due to the spatial climatic differences and the anthropogenic trend in the observations. We accept this bias since the grid cell with the largest effect only shows an increase in standard deviation by 7% for temperature, 2% for downwelling longwave radiation, and 0.1% for precipitation and downwelling shortwave radiation. Since experiment EXP1 only involves randomization in time but not space, the error in this simulation is even smaller.

Regarding the idealized domain (EXP2 and EXP3), to systematically assess the model's response to a large range of inputs, we rescale the precipitation input: We let mean annual precipitation (MAP) vary linearly from 0 to 3800 mm/year in what would normally be the longitudinal dimension of the model domain and vary the seasonality from 0 to 2.8-times the observed seasonality in the latitudinal dimension (see Section S2). Due to the randomized input, the distributions of temperature and the two radiative fluxes are homogeneous within the simulated domain and are not further manipulated. We also impose sandy loam as the only, spatially uniform soil type. Consequently, any spatial differences in the vegetation will be caused by the different precipitation input.

TABLE 1 | List of simulations with different versions of LPJmL and the reduced model. LPJ-CN refers to the model with coupled dynamics of carbon pools *C* and population *N*, LPJ-C refers to the carbon-only model with fixed *N*, and LPJ-N refers to the population-only version with prescribed pools *C*. Subversion names including "Ei" involve interactive establishment *est*, while "Er" refers to prescribed establishment with randomized years. A1 stands for enabled adjustment and A0 for disabled adjustment. Variables *P* and *T* stand for precipitation and temperature, respectively. All other variables prescribed in EXP4-11 are obtained from the output of EXP3. SM stands for soil moisture and C_{ass} for total assimilated carbon. All variables listed in the column "input" have been randomized. See Section 2 for details on the model variants and experiment setups.

EXP	Version	Input	Modifications	Figures
Experiments with the full LPJmL model to reveal resilience patterns				
1	LPJmL	*P*, *T*, radiation	Default: full LPJmL model with all 11 PFTs, domain: Meso and South America	Figure 1, Figures S5 and S6
2	LPJmL	*P*, *T*, radiation	Default: full LPJmL model with all 11 PFTs	Figure 2a
3	LPJmL	*P*, *T*, radiation	Full LPJmL model but with tropical broadleaved evergreen trees as the only PFT	Figures 2b and 3, Figure S7
Experiments with the reduced LPJmL model for separating population and carbon dynamics				
4	LPJ-CN (=LPJ-CN-EiA1)	C_{ass}, SM	Standard reduced model	Figures 4 red, 5b red, 6e–h, 7a and 8, Figures S4, S8 blue, S9 and S10
5	LPJ-C	C_{ass}, SM, *N*	*C* pools only, fixed *N* (no population dynamics), fixed mortality as loss term for pools	Figures 4 blue and 7b–d, Figure S8 orange
6	LPJ-N (=LPJ-N-EiA1)	*L*, *R*, *S*, *H*	Prescribed carbon pools, population dynamics interactive	Figures 5a red and 6a–d, Figure S8 green
Experiments with the reduced LPJmL model for testing mechanisms that affect population dynamics				
7	LPJ-N-ErA1	*L*, *R*, *S*, *H*, est	Prescribed carbon pools, population dynamics interactive, randomized establishment	Figure 5a blue
8	LPJ-N-EiA0	*L*, *R*, *S*, *H*	Prescribed carbon pools, population dynamics interactive, no adjustment	Figure 5a yellow
9	LPJ-N-ErA0	*L*, *R*, *S*, *H*, est	Prescribed carbon pools, population dynamics interactive, randomized establishment, no adjustment	Figure 5a black
10	LPJ-CN-ErA1	C_{ass}, SM, est	Randomized establishment	Figure 5b blue
11	LPJ-CN-ErA0	C_{ass}, SM, est	Randomized establishment, no adjustment	Figure 5b black

2.2 | Building a Reduced LPJmL Model

To facilitate interventions within the model and explore the role of different mechanisms in resilience changes, we developed a reduced version of the LPJmL model, which represents parts of the full model and is implemented in Python. The advantage of rebuilding parts of the model is that we can run the reduced model as a stand-alone model, that is, without running the rest of the model code, and modify its structure. Variables not simulated by the reduced model are prescribed from the full LPJmL. The reduced model describes the dynamics of vegetation carbon pools and population dynamics with a time step of 1 year, for one single tree type (here: tropical broadleaved evergreen trees). Similar reduced models have also been constructed for a number of other DGVMs (Luo et al. 2017). We constructed the relevant equations by following the procedures in the full model's code and the available documentations (Sitch et al. 2003; Schaphoff, von Bloh, et al. 2018). For a more detailed model description and the code, see Section S3 and Section 4.1.

We have assured in extensive tests that our reduced model reproduces the dynamics of the underlying part of the full original model. For all individual processes, the reduced model and LPJmL produce numerically identical results. However, due to error growth when coupling all components together, the default reduced model may slightly deviate from the full LPJmL model and occasionally develop numerical instability. Despite this, the

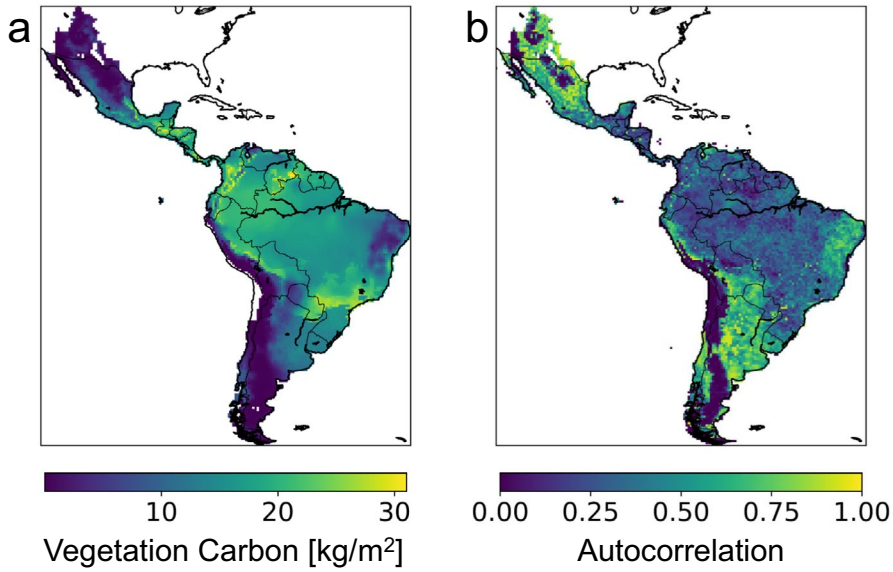

FIGURE 1 | Vegetation carbon in LPJmL when forced by randomized daily observations in the domain of Mesosouthamerica (EXP1 in Table 1) (a) time mean and (b) autocorrelation (lag: 10 years).

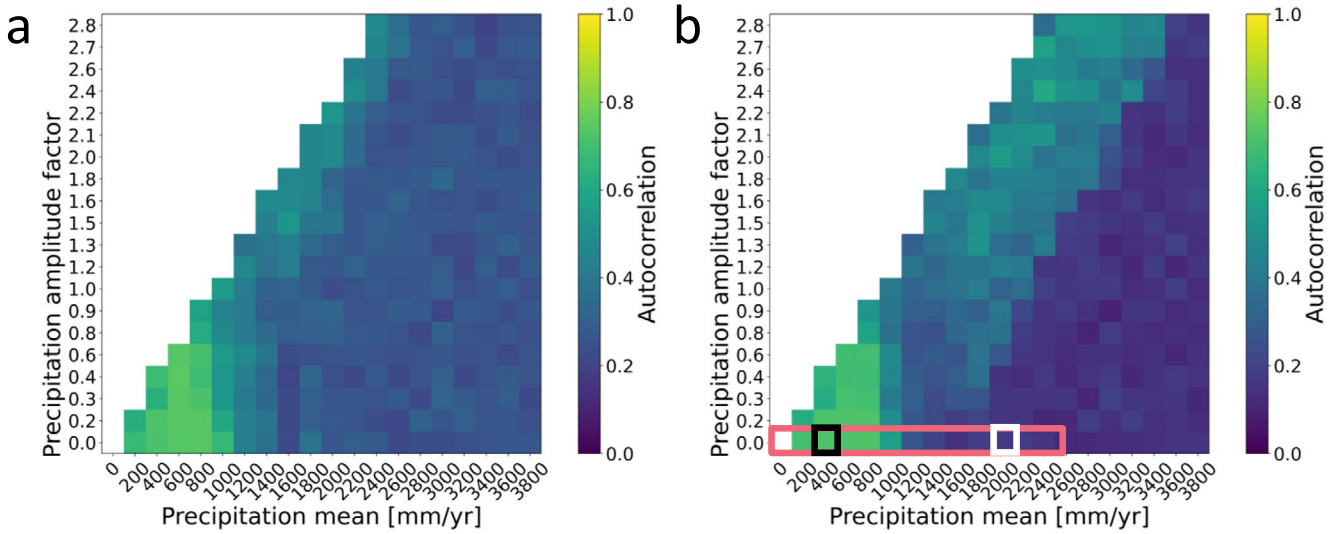

FIGURE 2 | Autocorrelation (lag: 10 years) of vegetation carbon in LPJmL. (a) Full LPJmL model with all 11 plant types (EXP2). (b) Same model but with tropical broadleaved evergreen trees as the only plant type (EXP3). The axes of each plot show mean annual precipitation and the amplification factor for scaling the annual cycle of precipitation as prescribed from the input data. The white and black grid cells are chosen for additional simulations (see the main text). The purple box shows the cross section used in Figure 3 and Figures S7 and S8.

overall behavior remains identical (see Figure S2). Correlations between LPJmL simulations and corresponding ones produced with the reduced model are typically above 0.99.

LPJmL simulates only one representative tree individual per plant type, with leaf carbon (L), root carbon (R), sapwood carbon (S), and heartwood carbon (H) in gC per individual. The fifth dynamic variable is the population density (N) in tree individuals per m^2. Hence, the vegetation carbon $\widetilde{C}$ in gC per m^2 is

$$\widetilde{C} = (L + R + S + H) \times N \quad (1)$$

The reduced model receives two variables as input, which we feed in from the original LPJmL model (Figure S3): The total allocated carbon in gC per individual tree per year, C_{ass} (computed from net primary productivity, reproduction costs, and quantitatively negligible debt fluxes which are carry-over effects from 1 year to the next in order to keep the carbon balance closed), and the relative soil moisture between 0 and 1. No atmospheric input variables are required for the reduced model because they act on the modeled variables only indirectly via the productivity. When forced by these two variables, the reduced model can reproduce the dynamics of the five state variables from the full LPJmL model, including dependent non-dynamic (diagnostic) variables such as foliage projected cover (FPC), leaf area index (LAI), crown area (CA), and tree height (h), which are updated several times a year based on empirical structural relationships (see Sitch et al. 2003 and Table S1). Every year, the model updates the population density

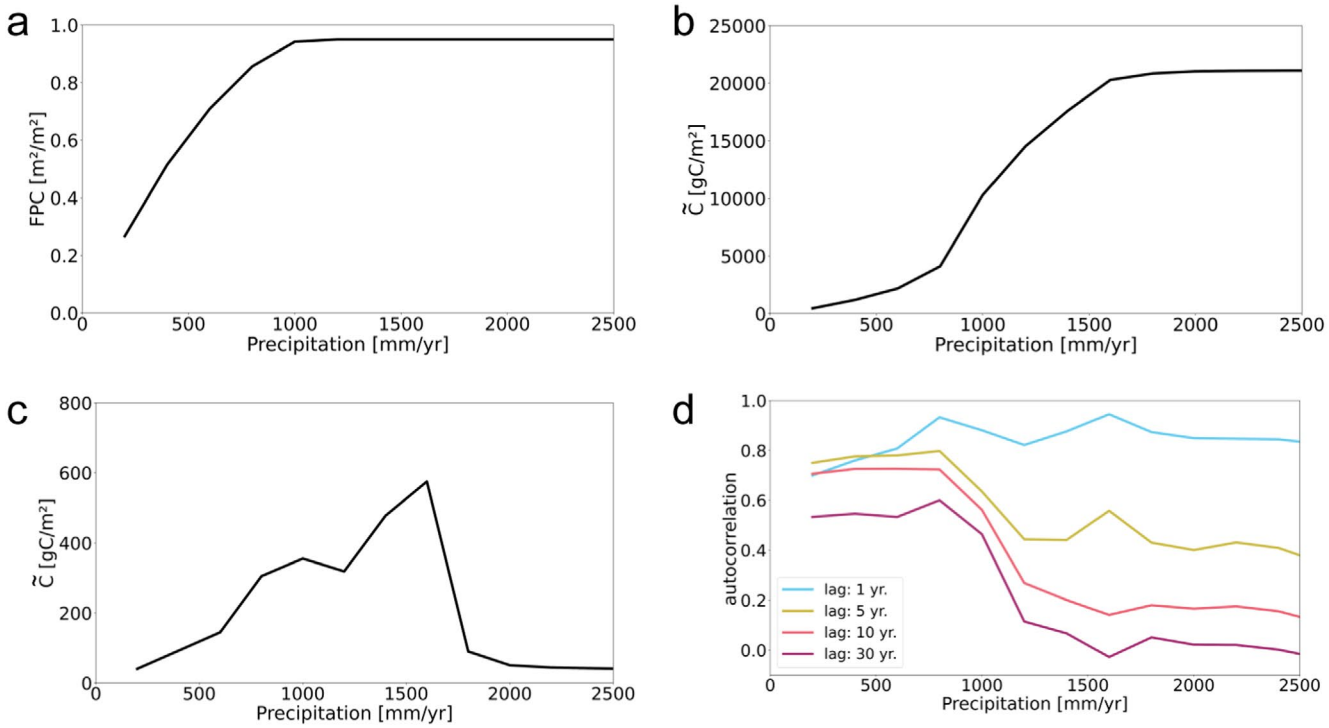

FIGURE 3 | Relationship between mean annual precipitation and (a) total foliage projected cover (FPC), (b) vegetation carbon $\widetilde{C}$, (c) standard deviation of $\widetilde{C}$, and (d) autocorrelation of $\widetilde{C}$ for four different lags, all in experiment EXP3, as a cross section shown as the purple rectangle in Figure 2b.

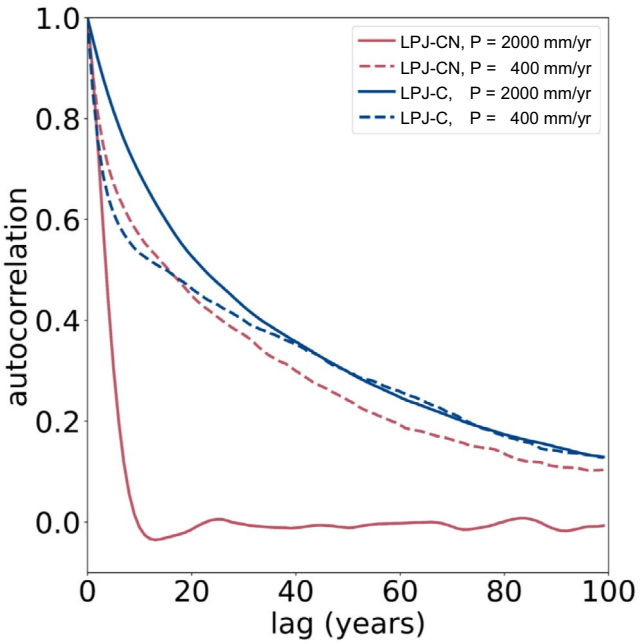

FIGURE 4 | Autocorrelation function of vegetation carbon in a wet climate (solid lines, white grid cell in Figure 2b) and dry climate (dashed lines, black grid cell in Figure 2b), for different versions of the reduced LPJmL model. Red lines: Default model LPJ-CN (EXP4), blue lines: Model with fixed population density, LPJ-C (EXP5). See Table 1 for different model versions and experiments.

based on the processes of tree mortality (Section S3.3), establishment of new saplings (Section S3.4), and an adjustment in case the trees cover more than the available grid cell area (Section S3.5). Mortality and adjustment are loss terms (negative or zero), whereas establishment is a source of trees (positive or zero). Each of the four individual carbon pools C_i is updated based on turnover (Section S3.1), allocation of assimilated carbon (Section S3.2), and a rescaling after the establishment of new trees (Section S3.4, Equation S5). Assimilation is the source term (typically positive), whereas the other two terms are negative or zero.

For a detailed description of the dynamics of vegetation carbon and population dynamics, see Table S1, Section S3, and previous model descriptions (Sitch et al. 2003; Schaphoff, von Bloh, et al. 2018). Note that we ignore the mortality from light competition, which in LPJmL occurs between growth-related mortality and establishment (steps 3 and 4 in Table S1), but only in some years, and only at grid cells with precipitation between 800 and 1800 mm/year. Since it had no effect on the results we discuss in this study, we omitted this term in the reduced model.

2.3 | Variants of LPJmL and the Reduced Model

Our results involve a variety of model versions that we name by using abbreviations that indicate which processes in the model have been modified (Table 1). Using the full LPJmL model, we perform one simulation for Meso and South America (EXP1) and two simulations for the idealized setup: One with all 11 PFTs (EXP2) and one using only tropical broadleaved evergreen trees as the only PFT (EXP3). Tropical broadleaved evergreen trees are the only PFT in all simulations except EXP1 and EXP2, that is, in all simulations with the reduced model.

All simulations discussed in the main part of this article used randomized input variables as explained in Section 2.1. This

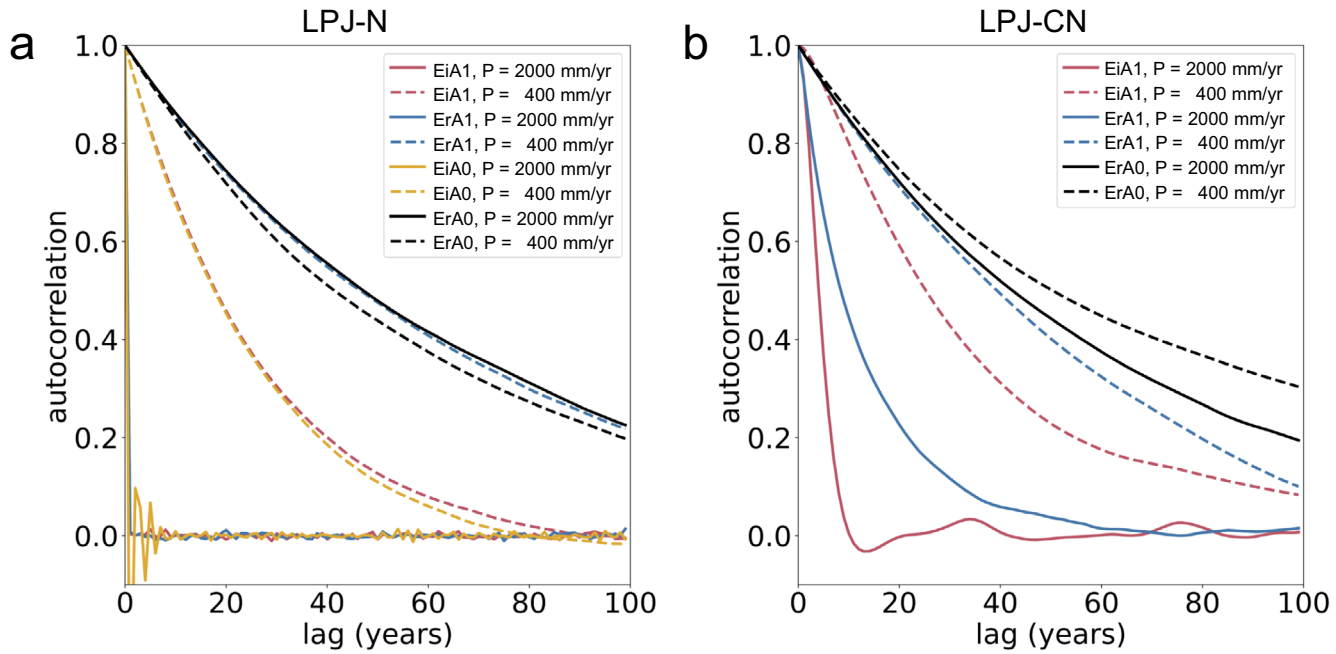

FIGURE 5 | Autocorrelation function of population density N in a wet climate (solid lines, white grid cell in Figure 2b) and dry climate (dashed lines, black grid cell in Figure 2b), for different versions of the reduced model. (a) Population-only version LPJ-N and (b) default model with fixed mortality LPJ-CN. Each color is a different model version, where Ei = interactive establishment (Equation S4), Er = randomized establishment read in from EXP3, A1 = adjustment active, A0 = no adjustment. See Table 1 for different model versions and experiments.

includes climate input and the input of assimilated carbon and soil moisture to the reduced model. The randomization of yearly productivity that is passed to the reduced model slightly decreases the autocorrelation of vegetation carbon (Figure S4) but has no major effects on our results. Moreover, all simulations with the reduced model (EXP4-EXP11) involve the simplification that we prescribe the mortality rate *mort* to a constant value of 0.015, which is a typical value also in the original model. This simplification does not qualitatively change any of our results (as an example, see Figure S4).

We generate three major variants of the reduced model that allow for a separation of different effects. The default reduced model, called LPJ-CN, is structurally identical to the full LPJmL model apart from the fixed mortality rate. Essentially, the dynamics of carbon pools involve a balance between allocation and turnover (Figure S3), while population dynamics are a balance between establishment and mortality and an adjustment for high cover fractions (Section S3, Table S1). Both are coupled via the establishment of new trees (Section S3.4, Equation S5). To separate carbon dynamics from population dynamics, we create two additional major versions of the reduced model. In the carbon-only version (LPJ-C), we set the population density N to its time-averaged value obtained from Experiment EXP3. In the population-only version LPJ-N, we prescribe carbon pools from EXP3 and only simulate population density.

Version LPJ-C involves one additional modification. In the full model, the establishment of tree saplings directly reduces the carbon stored in the average individual tree (Equation S5) and hence acts as a sink term for individual-based carbon pools (L, R, S, and H), whereas tree mortality leaves these pools unchanged. Running LPJ-C without population dynamics would lack this sink term and hence lead to carbon storage far outside the plausible range. To prevent this, we include a linear sink term that reduces all carbon pools with a dummy mortality rate mort_C of 0.015 per year, that is, the same rate as the mortality rate in the full model. Version LPJ-C thereby structurally resembles most DGVMs used in CMIP models, which typically do not include population dynamics.

The population-only version LPJ-N follows a similar approach as LPJ-C: We prescribe carbon pools from EXP3 and simulate population density. In contrast to the carbon-only version LPJ-C, where we fixed N at a constant value, in the population version LPJ-N, we prescribe yearly (randomized) values of the carbon pools instead of the time mean. This is necessary because otherwise the model would not exhibit any variability from which we could compute autocorrelation.

For both the population-only model LPJ-N and the default version LPJ-CN, we also create three subversions, where the interactive computation of the tree establishment rate (Section S3.4, Equation S4) and the adjustment of population density N (Section S3.5) can be switched on or off. Regarding establishment, we distinguish interactive establishment (Ei), as used in the default model, from randomized establishment (Er), where we read in the establishment rate from a randomly selected year in EXP3. Regarding adjustment, we distinguish enabled adjustment (A1) from disabled adjustment (A0). A0 means that the adjustment step is skipped when running the model.

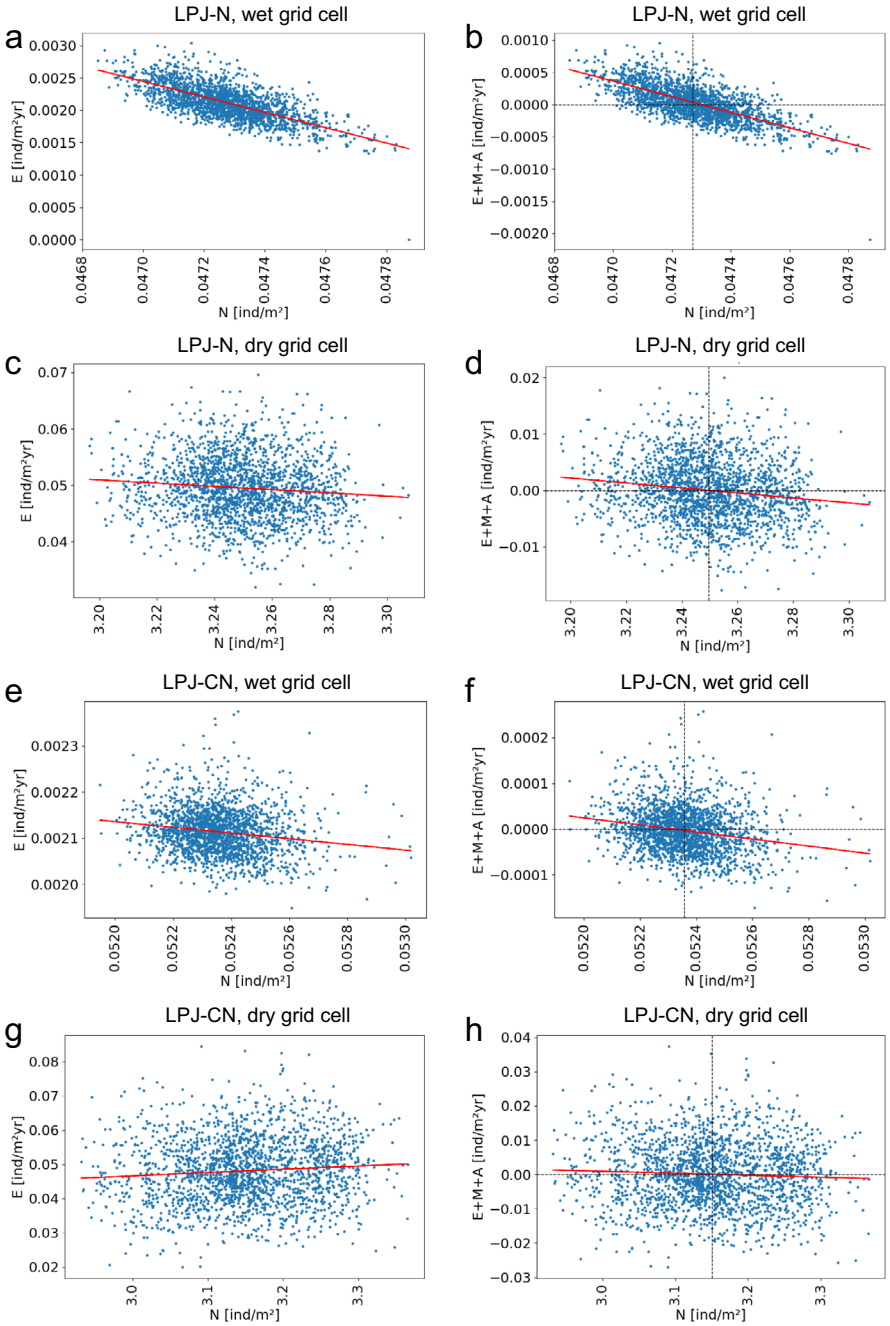

FIGURE 6 | Relationship between current population N and the establishment of new trees (E) in the next time step (a, c, e, g), and the total change of N due to establishment, mortality, and adjustment ($E+M+A$) (b, d, f, h), respectively. Hence, E stands for establishment *est* (Equation S4), M for mortality mort (Equation S3), and A for the effect of the adjustment on N (Section S3.5). Each dot represents one time step of 1 year in time series of 2000 years in length. Red lines are the linear regression line of this data. Black dashed lines denote zero change (horizontal lines) and the time average state (vertical lines). Model versions used are the default LPJmL model with fixed mortality (LPJ-CN) and the model with prescribed carbon pools (LPJ-N). "Wet" and "dry" grid cell in the titles refer to the white and black grid cell highlighted in Figure 2b, respectively.

3 | Results

3.1 | Biomass Autocorrelation in LPJmL

To demonstrate how different climates affect vegetation carbon variability (specifically, its autocorrelation) in LPJmL, we first analyze the quasi-realistic simulation EXP1 for Meso and South America. In moist tropical climates, the only relevant tree types are tropical broadleaved evergreen trees and tropical broadleaved raingreen trees, with the first typically dominating (Figure S5). In the Amazon, an even larger fraction of broadleaved evergreen trees would be more realistic, which points to a known bias in LPJmL (Sakschewski et al. 2021), but does not affect our results, as they do not depend on the composition of tree types (see below). Overall, the distribution of vegetation carbon is in good agreement with observations (Schaphoff, Forkel, et al. 2018), despite the randomization of the climate input. It becomes obvious that in places where vegetation carbon is large, its autocorrelation tends to be small (Figure 1). Climate variability does not impose this effect because, as described in

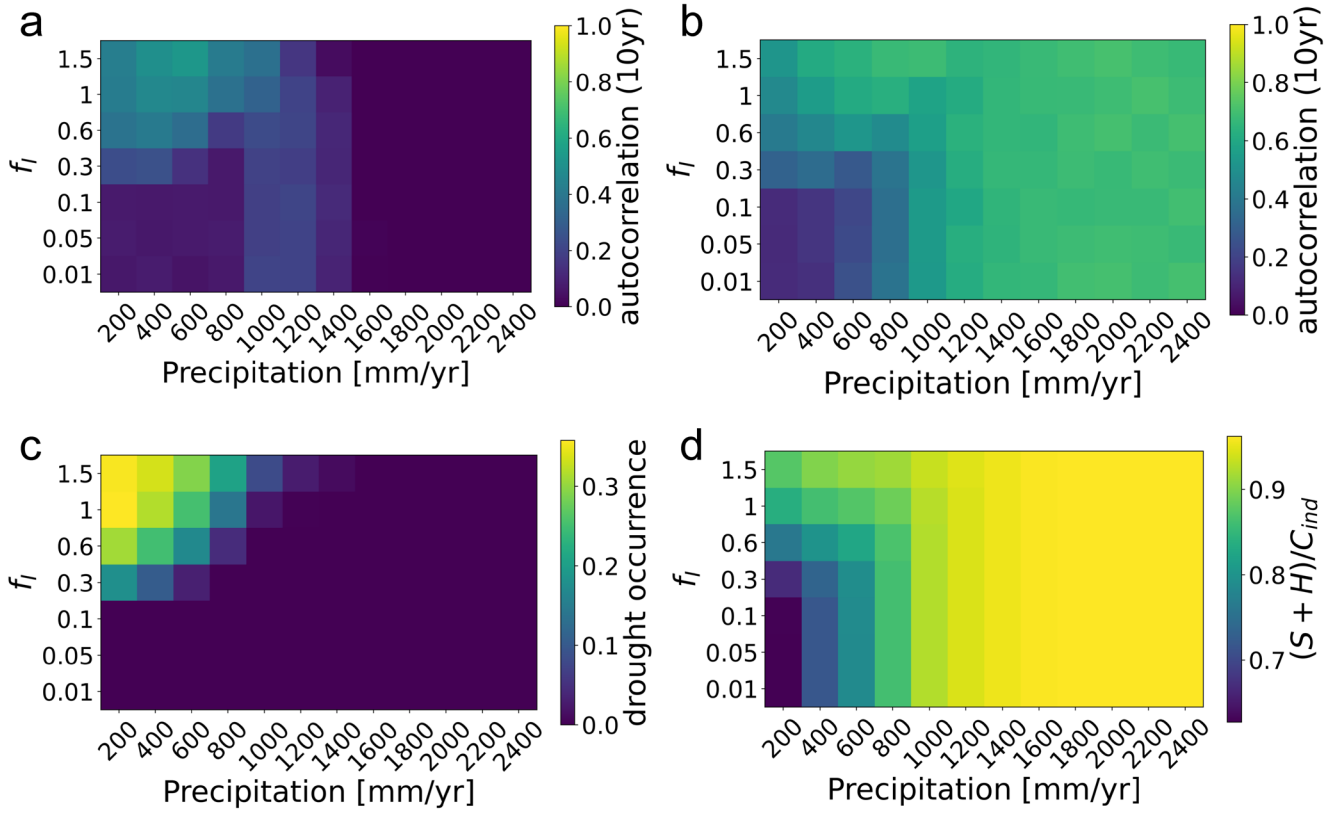

FIGURE 7 | Effect of scaling the variance of input variables in LPJmL in (a) the default reduced model LPJ-CN (EXP4) and (b–d) the model with fixed population density and mortality-based loss term, LPJ-C (EXP5). (a) and (b) show autocorrelation (lag: 10 years) of vegetation carbon, (c) the fraction of years with drought stress, and (d) the fraction of sapwood and heartwood relative to the total vegetation carbon. All results are obtained with a completely suppressed annual cycle (purple cross section in Figure 2).

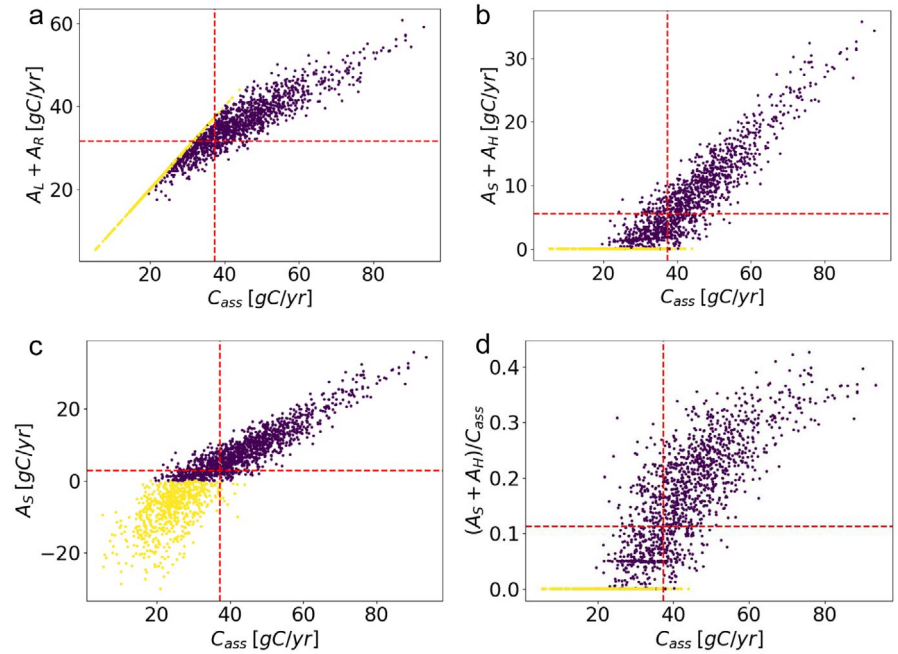

FIGURE 8 | Carbon allocation in the default model (LPJ-CN, EXP4). Horizontal axes show the total assimilated carbon in a year. Vertical axes show the sum of carbon allocated to leaves and fine roots (a), the sum of carbon allocated to sapwood and heartwood (b), to sapwood alone (c), and the fraction of carbon allocated to sapwood and heartwood (d). Each point represents 1 year from a 2000-year time period at the black (dry) grid cell shown in Figure 2. Years shown in yellow are years with drought stress where the total allocated carbon is too small to support the current sapwood (see Sitch et al. 2003 and Section S3.2); all other years are shown in purple. Red dashed lines show the time mean of the data on both axes.

Section 2.1, the meteorological input is randomized and hence has zero autocorrelation. The pattern is confirmed when plotting climate input variables against the autocorrelation of vegetation carbon: Small MAP is associated with higher autocorrelation, whereas mean annual temperature does not have a clear effect (Figure S6).

Nian et al. (2024) have shown that vegetation carbon in LPJmL exhibits a threshold determined by MAP and precipitation seasonality (but less so by fire), and that slowing down (e.g., measured via increasing autocorrelation) can occur when approaching this threshold. This result can also be seen in simulations with our idealized setup: Grid cells with low MAP tend to show substantially higher autocorrelation than wetter grid cells (Figure 2). When using a single PFT, the difference between high-autocorrelation dry grid cells and low-autocorrelation wet grid cells is even more apparent (Figure 2b). This shows that the composition of PFTs is not relevant for explaining this pattern, which is why we only discuss simulations with a single PFT in the following.

It also becomes apparent that the MAP threshold, where slowing down sets in, is higher where seasonality is larger (Figure 2). As pointed out by Nian et al. (2024), higher seasonality overall implies stronger water limitation due to the existence of a dry season. In the following, we aim to explain why autocorrelation increases with decreasing MAP. To this end, we pick a range of MAP values with zero seasonality (shown as the purple rectangle in Figure 2b), as well as a single grid cell with high MAP (2000 mm/year) and a grid cell with low MAP (400 mm/year), marked as the white and black grid cells in Figure 2b, respectively. Due to the absence of seasonality, the MAP threshold where autocorrelation increases is smaller than in the more realistic simulations EXP1 or EXP2, but for the reasons explained above, it is caused by the same mechanism.

When looking at the purple cross section, we find that the FPC fraction of the trees gradually increases with precipitation and saturates at its maximum value of 0.95 at around 1000 mm/year (Figure 3a). The carbon pools only reach a plateau at a higher MAP value (Figure 3b), when trees reach their largest size. Plotting the standard deviation of vegetation carbon along the range of MAP values reveals that this indicator is largest between approx. 1000 and 2000 mm/year (Figure 3c). In principle, this result is what can be expected from the nonlinear relationship shown in Figure 3b. In order to obtain a large variance, either the climate variability needs to be large or the vegetation biomass needs to be sensitive to climate. The climate variability here is dominated by MAP because fluctuations in temperature and radiation are small. In our experiments, the standard deviation of precipitation is proportional to MAP by design and hence becomes small for small MAP. Moreover, biomass is most sensitive to precipitation between approx. 800 and 1500 mm/year (Figure 3b). Consequently, we find the highest variance on the high end of the intermediate MAP regime, where MAP variability and the sensitivity of $\widetilde{C}$ to MAP are both large. We therefore propose that increasing variance can indicate an increased sensitivity of the rainforest's biomass to climate change.

The cross section of autocorrelation again clearly shows the pronounced slowing down for reduced precipitation (Figure 3d). This result qualitatively agrees with the relationship found in observations (Verbesselt et al. 2016; Boulton, Lenton, and Boers 2022; Smith and Boers 2023a) (Figure S1). However, in the model, differences in autocorrelation only emerge beyond a lag of 1 year (Figure 3d), whereas observational studies used monthly time lags (which is below the model's annual time step). We come back to this difference in the discussion section. In the remainder of this study, we will discuss what explains the dependency of autocorrelation on precipitation in the reduced model.

3.2 | Separation of Carbon and Population Dynamics

To identify the processes that give rise to the contrasting autocorrelation—and hence characteristic time scales—in dry and wet climates, we now assess the sensitivity of this autocorrelation to structural changes and parameter variations in the reduced model described in Section 2.2 and Section S3. As mentioned above, the autocorrelation pattern persists when randomizing the climate input in LPJmL, and when using only a single tree type. It also persists when driving the reduced model LPJ-CN with randomized input of assimilated carbon and soil moisture (Figure S4). Therefore, neither land–atmosphere feedbacks nor feedbacks between carbon pools and productivity are needed to understand the mechanisms behind the autocorrelation pattern.

To further reduce complexity and isolate the mechanisms behind the autocorrelation pattern, we now run the carbon-only version LPJ-C where population dynamics are turned off (EXP4), prescribing the total assimilated carbon and soil moisture from the full model LPJmL (EXP3; see Table 1 and Section 2.2). As a result, the distinct difference of autocorrelation between dry and wet grid cells disappears (Figure 4 and Figure S8). We obtain similar results if we do not set population density to a constant value but read it in (again in a randomized way) from the default run EXP3 (not shown). Moreover, we can also scale all increments of N in all steps where N is updated in the default model by a factor f_N. This scaling parameter allows us to make a gradual transition between the default model and the carbon-only model, where N is constant. Reducing f_N toward values close to 0 indeed results in a large and homogeneous (climate-independent) autocorrelation, as found in LPJ-C (Figure S9). These results reveal that the population dynamics are key to explaining the different autocorrelation values in wet and dry climates in the model. Only capturing carbon dynamics by allocation as a source term and linear relaxation as a sink term (as typically done in CMIP models) is too rigid an approach to create any substantial differences in autocorrelation for different climates, at least for the range of climate inputs we analyze (we will discuss an exception to this finding in Section 3.4).

It should be noted that in the default simulation with LPJmL as well as the reduced model, the carbon per individual tree does show a distinct autocorrelation difference between wet and dry climates, like the carbon pools per unit area. This signifies that the pattern is not simply imposed by the vegetation dynamics when multiplying individual-based pools and population density N (Equation 1), but that the autocorrelation of population density N also affects the autocorrelation of the carbon pools due to the interaction of these variables in the model. The process by

which this happens is the rescaling of pools after tree establishment (see Table S1 and Equation S5), which is the only procedure where carbon pools are directly affected by N in the model.

3.3 | Effect of Population Dynamics on Autocorrelation

The next step is to further reveal the mechanism by which the population dynamics shape the autocorrelation pattern shown in Figures 2b and 3d. To this end, we use the population-only version of the reduced model (LPJ-N, EXP6 in Table 1). This setup again reproduces the dichotomy of slow recovery in dry climates and fast recovery in wet climates (Figure S8, Figure 5a, red lines), confirming our finding that population dynamics indeed cause this pattern in vegetation carbon dynamics in the full model. The factors controlling the time scale of N are the mortality rate, the establishment rate, and the adjustment. In principle, the mortality always acts as a stabilizing term because larger N results in a larger mortality-related loss (Equation S3). In the full LPJmL model, the interactive mortality (Equation S2) implies higher mortality in drier climates, in line with expectations and observations (Bauman et al. 2022; McDowell et al. 2018). This tends to decrease the autocorrelation at dry grid cells relative to wet grid cells, opposite to the effect we aim to isolate here. In the reduced model, mortality is fixed as explained in Section 2.

What remains as possible explanatory mechanisms are the establishment and adjustment. The establishment rate (Equation S4), which increases N, itself decreases with increasing FPC_{woody} due to the limited space trees have available once the area is completely covered by the tree canopy. In turn, FPC_{woody} increases with N because more trees tend to cover more area. Consequently, there is a negative (and hence stabilizing) feedback loop between population N, cover fraction FPC, and establishment *est*, which is most effective when the available area is completely covered by trees (i.e., where FPC_{woody} is close to FPC_{max}), corresponding to a beneficial climate. The factor controlling the strength of the negative feedback cycle involving FPC, *est*, and N is the expansion of area coverage per additional tree (effect of N on FPC). In favorable climates, trees are larger than in harsh climates; hence, each additional tree covers a significantly greater area, impeding the establishment of new trees more effectively than in arid climates.

To illustrate the role of the establishment feedback and the linear stability of the dynamic equation for N (including all three terms for mortality, establishment, and adjustment), we can regress the yearly increments of N associated with the different sub-processes onto N (Figure 6). Both the establishment (Figure 6a) as well as the total increment (Figure 6b) are negatively correlated with N, indicating a stable system. At the dry grid cell, the scatter around this slope is much larger, indicating a less persistent restoring force. At the same time, the situation with high area coverage also enforces an adjustment of FPC and N in order to stay below FPC_{max} (see Section S3.5), which results in a sudden (memory-free) shift to smaller values of N (and thereby $\widetilde{C}$). Figure 3a shows that the threshold where the adjustment process sets in is around 1000 mm/year, which coincides with the transition from high to low autocorrelation (Figure 3d). This effect co-occurs with the negative establishment feedback in the wet climate regime and also has the potential to reduce autocorrelation. As the two effects are not separable from a diagnosis of the full model alone, we compare results for a set of subversions of LPJ-N (EXP6 to EXP9) where (i) the establishment feedback cycle can be broken by randomizing the establishment rate, and (ii) the adjustment can be disabled, hence allowing the tree canopy to cover more than 95% of the area.

Interestingly, already in the population-only setup with establishment and adjustment in their default representation, autocorrelation is essentially zero at the wet grid cell (Figure 5a, red bold line). Each year, the beneficial climate tends to increase N further, but the area coverage FPC reaches the threshold FPC_{max}, where both N and FPC are reset by the adjustment procedure. This results in time series with very small autocorrelation. In contrast, at dry grid cells, autocorrelation is substantially larger (red dashed line). Because of the removal of a stabilizing feedback, randomizing the establishment increases the autocorrelation at the dry grid cell (blue dashed line in Figure 5a). Disabling the adjustment process alone does not affect the results (yellow lines versus red lines in Figure 5a). In both cases, however, the difference between the wet and dry grid cells remains. This situation only changes when breaking the establishment feedback and disabling the adjustment at the same time (Figure 5a, black lines). In this case, the autocorrelation functions are almost identical at the wet and at the dry grid cell, with high autocorrelation everywhere, since it is only the (fixed and universally constant) mortality rate that stabilizes the system. Obviously, both mechanisms (establishment feedback and adjustment) are responsible for the autocorrelation difference in the default model, in the sense that either of them suffices to reproduce this pattern. While these results are obtained with the population-only model LPJ-N, we repeat our analysis with the default model LPJ-CN. We obtain essentially the same results, with the minor difference that there is now also autocorrelation at the wet grid cell due to the enabled carbon dynamics (Figure 5b). Switching off the adjustment alone turned out to make the model unstable, creating large oscillations with a time period of several years. A slight indication of such numerical instability also occurs in the population-only model (Figure 5a, continuous solid yellow line at low lags). Figure 5b therefore omits the EiA0 subversion. We note that numerical instability has also occurred in subvariants of the reduced model not shown in this paper and also occurs when forcing LPJmL or the reduced model with constant environmental conditions. These numerical instabilities indicate that a 1-year time step is at the limit of acceptable numerical resolution. This, together with the fact that the cutoff-like adjustment process is needed at all in LPJmL, lets us conclude that increasing the temporal resolution of vegetation dynamics in LPJmL might improve the realism of the model.

We have now explained how the autocorrelation of N is shaped by mortality, establishment, and adjustment and also how it in turn affects the autocorrelation of the individual-based carbon pools in LPJmL. However, the total vegetation carbon per grid box area is the product of individual-based pools and N (see Equation 1). In principle, it is unclear what the autocorrelation function of the product of two autocorrelated processes looks like. Apart from the individual autocovariances, the means, variances, and the covariance between the two variables also play a role. To track how the autocorrelation pattern we found

in the dynamics of N directly carries over to vegetation carbon per area, we therefore explicitly compute the 10 different terms contributing to the covariance (see Equation S9) and the 7 terms contributing to the variance (Equation S8) of the product $C*N$ (since autocorrelation is defined as the ratio between autocovariance and variance), using equations derived in Bohrnstedt and Goldberger (1969). We find that the only terms with a relevant contribution involve the autocovariances (in the numerator) and variances (in the denominator) of C and N, while higher order effects are negligible (Figure S10). We conclude that the autocorrelation of vegetation carbon in the model can be understood via the mechanisms shaping the individual autocorrelations of N and C that we discussed above.

3.4 | Role of Climate Variability and Allocation

We now shift our attention to an additional process that has not been extensively discussed in the previous sections: the allocation of carbon to the four vegetation carbon pools. This module is more complex than the rest of the reduced model and exhibits nonlinear behavior between climate input and vegetation carbon dynamics (see Section S3.2).

To reveal the relevance of this nonlinear behavior for the autocorrelation of vegetation carbon, we again apply the default reduced model (LPJ-CN) and now scale the variability of the input variables (here soil moisture and productivity) by a fixed factor f_I, using a range of values from 0.01 (corresponding to reducing the standard deviation of input variables to 1%) to 1.5 (50% increase). We do this by first computing the anomalies (relative to the time mean) from EXP3, scaling them by f_I and then adding the anomalies back on the mean, hence conserving the correlations and autocorrelations. By suppressing the total variability in this way, the nonlinearity of the allocation module, which involves several case distinctions (see Section S3.2), is revealed. Figure 7a shows that as a consequence, the high autocorrelation that occurred at dry grid cells in the default model ($f_I=1$) decreases when muting the variability, until it becomes even smaller than at the wet grid cells. To isolate this effect, we repeat the simulations with the model version LPJ-C, where population density is constant in time (Figure 7b). In this version, autocorrelation at wet grid cells is much higher than in LPJ-CN because the negative feedback loop involving establishment and adjustment discussed in Section 3.3 is disabled. However, the effect of climate variability on the autocorrelation at dry grid cells is still present (Figure 7b). Consequently, this effect cannot be attributed to population dynamics, nor is it related to turnover fluxes (the sink terms of the living carbon pools), because turnover is linear (see Equation S1 in Section S3). We hence investigate how climate variability affects the allocation of carbon to the four different pools, using the default reduced model LPJ-CN, though results are similar in other versions. Figure 8 illustrates this for the grid cell shown in black in Figure 2b, with no variability scaling ($f_I=1$). In years with beneficial climate and high productivity (purple dots), the allocation fluxes to the fast pools, that is, leaves, and fine roots (Figure 8a), and to the slower pools, that is, sapwood and heartwood (Figure 8b), are both proportional to the total allocated carbon. Direct allocation to heartwood is then zero; its only source term is the turnover of sapwood, and its only sink term is the rescaling after the establishment of new trees.

In contrast, in years with adverse climatic conditions and low productivity, all allocated carbon is required to maintain leaves and fine roots. As there is more sapwood than is needed to support the small leaf area, carbon is redistributed from sapwood to heartwood. Hence, allocation to sapwood in these years is negative (Figure 8c), allocation to heartwood is positive, and the sum of both is zero (Figure 8b,d). This situation is what Sitch et al. (2003) described as "years of stress" in the subsection "Allocation" of their Methods section. It occurs in our simulations because of drought. We have marked the data from these years in yellow in Figure 8. In the simulations with scaled variability, the fraction of years with such drought events is particularly high for scaling factors where the autocorrelation is also high (Figure 7c). We propose that this effect can be understood as follows: Under dry conditions, the allocated fraction to sapwood S and heartwood H is zero because total productivity C_{ass} is too small for the tree to grow (Figure 8b,d). This changes in years with higher productivity, where there is a net positive flux of carbon to the slow pools S and H. This nonlinearity implies that negative and positive anomalies in productivity do not cancel out in their effect on the allocated fractions, which hence depend not only on the mean total productivity C_{ass}, but also on its variance. The larger the variance of A, the higher the allocated fraction to S and H, which can indeed be diagnosed in the simulations with scaled variance (Figure 7d). This is different from wet grid cells where years with positive and negative anomalies of A cancel out in their effect on the allocation to different pools. The effect of a larger share of pools S and H, however, directly implies a slower turnover rate of the total vegetation carbon. While leaves and fine roots are lost via turnover (with a time scale of 2 years in case of tropical evergreen trees, see parameters f_L and f_R in Table S2), the turnover carbon from the sapwood pool is moved to heartwood and hence remains part of the vegetation carbon. Heartwood is only reduced through the establishment of new trees, which lowers the proportion of heartwood (H) in the average tree represented by the model. As a consequence, woody carbon has a much longer timescale than carbon in leaves and fine roots, and therefore a larger share of these slow pools increases the residence time and hence the autocorrelation of vegetation carbon.

4 | Discussion and Conclusions

Having scrutinized the mechanisms that determine variance and autocorrelation of vegetation carbon in LPJmL, we now reflect on the realism of the results and the implications for the interpretation of resilience trends derived from observations and other models in general. The changes in variance we find are straightforward to explain in principle and consistent with previous findings (Boulton, Good, and Lenton 2013): In a regime where the sensitivity to climate is high (which occurs in LPJmL at precipitation levels around 1000 mm/year), the same climate variability leads to a larger variance in carbon pools.

The autocorrelation pattern, however, is much more intricate. We have shown that the dichotomy of low resilience/slow recovery (i.e., large autocorrelation) in dry climates versus high resilience/fast recovery (i.e., small autocorrelation) in wet climates in LPJmL is determined by population

dynamics, namely, the fact that recovery in the wet climate regime is faster due to the negative establishment feedback and the adjustment process. While the adjustment effect is obviously a numerical feature due to a too large time step; this process works only in conjunction with the negative establishment feedback, as shown in Section 3.3. In their essence, both parameterizations represent the fact that establishment is reduced when less open space is available for seedlings, resulting in a negative (stabilizing) feedback and faster recovery from perturbations. In other words, in a dense forest, where light and space are the limiting parameters, gaps in the canopy lead to a relatively quick recovery via the growth of new trees, which is possible due to the high potential NPP in such a beneficial climate. On a fundamental level, this is arguably a plausible mechanism, which agrees with the observational studies mentioned above (Poorter et al. 2016; Verbesselt et al. 2016; Smith and Boers 2023a). The model result, however, is questioned by the fact that LPJmL only simulates one single average tree per cell instead of an actual succession. To corroborate our results, it would hence be helpful to repeat similar simulations with a gap model that distinguishes age cohorts. Also, the result may hinge on the assumption that allocations to growth, survival, and reproduction are reliably modeled.

Related to this, as the second important factor besides population dynamics, we indeed found that the carbon allocation scheme affects the autocorrelation of vegetation carbon. As previous studies also point out, the more carbon is stored in long-lived plant organs like sapwood or heartwood, the longer its residence time, and the longer the recovery time of trees [e.g., Song, Zeng, and Li 2016]. Therefore, in order to capture carbon dynamics adequately with models, it is important to implement an allocation module that is realistic under a range of climatic conditions, including inter-annual variability. The approach in LPJmL goes back to the "pipe model" (Shinozaki et al. 1964a, 1964b), which is based on observed linear relationships between trees' sapwood cross section and leaf area. While this model is theoretically supported by observations, it remains an idealization (Lehnebach et al. 2018), and it may be particularly problematic to use such empirical structural allometric relationships to infer a tree's response to drought stress. Such empirical relationships are also problematic when running the models into very different climate conditions with high CO_2. Schippers et al. (2015) evaluated three different allocation hypotheses in a tree growth model: fixed allocated fractions, the pipe model, and a hierarchical approach where allocation follows a hierarchy of priorities that are crucial for survival. They found that the pipe model compared particularly poorly to observed fluctuations in tree rings, while the hierarchical scheme performed best. Our results are hence an additional argument for improving allocation schemes in DGVMs. As shown in Section 3.4, the allocation scheme in LPJmL leads to increased autocorrelation (implying lower resilience) in climates with larger variability. This result cannot be unambiguously confirmed by observations. However, Smith and Boers (2023a) concluded that resilience is indeed lower in regions with more pronounced inter-annual precipitation variability. In contrast, Verbesselt et al. (2016) did not find a clear relationship between autocorrelation (of NDVI, not biomass) and precipitation variability. Interestingly, Ciemer et al. (2019) found that vegetation resilience is larger in regions with larger precipitation variability (in terms of the coefficient of variation). However, their resilience measure was the volume of the attractor basin as constructed from observed tree cover distributions, which merges local stability ("engineering resilience") with ecological resilience. It therefore remains to be seen whether these differences to our results are due to insufficiencies of LPJmL to simulate carbon allocation realistically (and/or to simulate multiple PFTs for the same biome that allocate carbon differently), or due to incomparable variables and resilience measures between the studies.

While the autocorrelation pattern seems to agree between LPJmL and observations, a closer look also reveals substantial methodological differences. First, the time scale analyzed in LPJmL (autocorrelation with 10-year lags in 10,000–50,000 model years) differs from the time scale in observational studies (typically monthly resolution of 40 year long satellite records). A more direct comparison is hindered by the lack of satellites before the 1980s, and the limitation that LPJmL does not resolve biomass dynamics on a time scale below 1 year. The fact that there is no longer time step in the model either and that we use randomized forcing implies that the autocorrelation we find at multi-year lags does result from interactions on shorter time scales. In this sense, the pattern of observed and modeled biomass dynamics in different climates may still be comparable to some extent, although we consider it plausible that other processes than population dynamics dominate the observed patterns.

Second, for the reasons discussed in Section 3.3, the precipitation threshold where autocorrelation is most sensitive in LPJmL coincides with the point where the FPC saturates at its maximum value (also see Nian et al. 2024). At MAP values above this threshold, there are no differences in autocorrelation, even though the biomass is still sensitive to precipitation (Figure 3). Insofar, autocorrelation and variance in LPJmL could be considered indicators of the sensitivity to climate change, but not "early warning" indicators. This differs from another version of LPJmL which does show increasing autocorrelation when approaching the MAP threshold from above (Nian et al. 2024). A possible explanation lies in the different model version used in Nian et al. (2024), which included more tree types (to allow for competition involving adaptable roots) and two more carbon pools, affecting the allocation. The latter suggests that the change in autocorrelation during drying may not be a robust result in models (at least in high precipitation regimes), despite the apparent similarity between LPJmL and observations.

Third, the observed biomass typically represents aboveground biomass only, because biomass below ground cannot be observed from space. LPJmL provides a proxy of aboveground biomass, which consists of all leaf and heartwood carbon, plus two-thirds of the sapwood carbon (i.e., excludes all root carbon and one third of sapwood carbon). Repeating our analyses with this proxy instead of total vegetation carbon does not make a substantial difference for our model results. Although this is assuring, it reminds us that satellite products like NDVI or VOD are not directly comparable to model

output. For example, the signal measured by the satellite may preferably originate from the tree canopy and the more exposed outer parts of trees, and less from heartwood within the tree, due to the attenuation of the radiation signal, which differs for different radiative bands (Forkel et al. 2023). The VOD is probably the satellite dataset best approximating aboveground biomass, but it is important to keep in mind that the microwave sensors used to measure VOD are mainly sensitive to water content, while DGVMs only simulate carbon storage. The water content in real trees can substantially differ between leaves, sapwood, and heartwood (Elsherif, Gaulton, and Mills 2018; Sohel et al. 2023) and also changes over time depending on environmental conditions, independently of the carbon storage (Borchert 1994; Dias and Marenco 2016). Since LPJmL suggests that the autocorrelation depends on the fraction of the different pools, it is vital for future studies to evaluate which properties of the vegetation are really represented in satellite records.

Fourth, we did not explicitly consider abiotic factors in our study other than climate, for example, soil type (Cole, Bhagwat, and Willis 2014) (though a comparison of EXP1, which includes heterogeneous soil types, and the other experiments shows no effect of the soil type), and we did not take into account that trees can locally adapt their traits to different conditions, a mechanism generally not implemented in DGVMs. While on the long time scales used in our simulations, space and time are interchangeable in the model, the real world might show a different response in transient situations. For example, biomass may decline under fast forcing, but recover due to adaptation on longer time scales (Sakschewski et al. 2016).

Fifth, we neglected processes like nutrient limitation and fire dynamics in our simulations, though these can be important at least for more realistic climate forcing. For example, Drüke et al. (2023) found a bistability in the Amazon when fire was activated in LPJmL when coupled to an Earth system model.

Overall, our results imply some recommendations for advancing models and observations in order to further close the complexity gap between the conceptual world of resilience indicators and the observed dynamics of tropical rainforests like the Amazon. Notably, it is vital to evaluate whether modeled quantities (specifically, resilience metrics) are consistent with observations, and whether both are consistent with the stochastic framework provided by dynamical systems theory. For example, Smith, Traxl, and Boers (2022) showed that the relationship between empirical recovery rates and observed autocorrelation and variance, inferred from VOD data, qualitatively agrees with the relationship expected from theory. Moreover, the fact that CSD-based estimates suggest higher resilience in situations of a water surplus compared to situations with water deficit Smith and Boers (2023a) can be considered an ecological proof of concept of the CSD framework. For optical sensors, Smith and Boers (2023b) demonstrated consistency between different CSD indicators at least for open, low-biomass vegetation types, although that study also showed that for denser vegetation cover, optical vegetation indices such as NDVI are not reliable. Observation-based studies should also be extended by more information about tree population dynamics which, according to our results, matters in particular on long time scales. Also, closely observing the carbon dynamics in individual tropical trees over time can help distinguish the signals on these local scales from the trends seen on a larger scale in satellite records.

Regarding the use of dynamic vegetation models, we conclude that DGVMs can point to processes that are worth being further investigated in order to improve our understanding of vegetation resilience, for example, using additional (ideally ground-based) observations. At the same time, systematic assessments of the stability of these models can also highlight their shortcomings, which need to be addressed before we can fully confirm the reliability of resilience indicators applied to satellite data. Specifically, our results imply that an improvement of allocation modules and resolving individual trees with structural dynamics and demographic processes would not only be beneficial for realistically simulating the future carbon cycle (Friend et al. 2014; Argles, Moore, and Cox 2022), but will also be necessary for an assessment of tropical rainforest resilience and its indicators. Area-averaged models without population dynamics, as typically used in CMIP6 models, may be structurally too limited to capture changes in forest resilience. Also, observations indicate that tree diversity matters (Hishe et al. 2021; Aguirre-Gutiérrez et al. 2022; Oliveira, Moore, and Dong 2022). The very limited number of tree types represented in DGVMs may be particularly problematic in this regard. Simulations similar to ours could therefore be repeated with models that represent more diversity, for example, by modeling different tree types or traits (Levine et al. 2016; Sakschewski et al. 2016), which would in turn require much more computational power and time.

Finally, the occurrence of CSD indicators like autocorrelation may change in a coupled climate-vegetation system. In this study, we have, on purpose, investigated the vegetation system in isolation, in order to work toward an improved understanding regarding which mechanisms play a role on different scales and in different components of the coupled system. The fact that we still find larger autocorrelation in dry climates supports scenario 1 outlined in the Introduction, namely, that no atmosphere–vegetation feedbacks are required to explain the observed relationships. Despite uncertainties regarding the magnitude of atmosphere–vegetation feedbacks in reality, and despite a large spread in the climate's response to deforestation in Earth system models (Boysen et al. 2020), it is likely that feedbacks are positive and thus potentially destabilizing. In the case of the Amazon, a loss of forest tends to make the regional climate drier and hotter due to a reduction in evapotranspiration (Eltahir and Bras 1996; Zemp et al. 2017; Bochow and Boers 2023) and impacts global climate through increased terrestrial carbon emissions, which would amplify the forest loss. The additional feedback would likely amplify CSD indicators in vegetation variables and potentially also atmospheric circulation and precipitation. As we find no indication of "false warnings" in the biosphere component (as has been found in other systems, e.g., sea ice, see Wagner and Eisenman 2015; Bathiany et al. 2016), our results do not contradict the hypothesis that such CSD-based warning signs would occur in the coupled system. The recently identified slowdown in basin-wide precipitation (Bochow and

Boers 2023) is an indication that a slowdown of the coupled atmosphere–vegetation system might indeed be happening.

We conclude that terrestrial vegetation models can help uncover processes that warrant further investigation to enhance our understanding of vegetation resilience, particularly through additional, ideally ground-based, observations. However, before we can fully understand and confirm the reliability of resilience indicators applied to satellite data, it is crucial to address the models' systematic limitations and the significant discrepancy in time scales between observed and modeled dynamics.

4.1 | Model and Analysis Code

Python code including the equations and parameter values for the reduced model, for running sensitivity analyses with this model, and for plotting the figures, is available on https://github.com/TUM-PIK-ESM/LPJ_resilience and zenodo (https://zenodo.org/records/14188139).

Author Contributions

Sebastian Bathiany: conceptualization, formal analysis, funding acquisition, investigation, methodology, project administration, software, visualization, writing – original draft, writing – review and editing. **Da Nian:** conceptualization, investigation, methodology, writing – review and editing. **Markus Drüke:** conceptualization, software, writing – review and editing. **Niklas Boers:** conceptualization, funding acquisition, methodology, project administration, supervision, writing – review and editing.

Acknowledgments

This is ClimTip contribution #3; the ClimTip project has received funding from the European Union's Horizon Europe research and innovation programme under grant agreement No. 101137601. S.B. and N.B. also acknowledge funding by the Volkswagen foundation. We are grateful for helpful discussions with Werner von Bloh, Boris Sakschewski, Maya Ben-Yami, Lana Blaschke, and Keno Riechers. S.B. is also grateful to Julia Falk, the Deutsche Bahn group, and the city of Moneglia for the inspiring work environment.

Conflicts of Interest

The authors declare no conflicts of interest.

Data Availability Statement

Model code that support the findings of this study are openly available in Zenodo at https://zenodo.org/records/14188139 and GitHub at https://github.com/PIK-LPJmL/LPJmL. Climate data is available from the Copernicus Climate Change Service (C3S) Climate Data Store (CDS) at https://doi.org/10.24381/cds.20d54e34.

References

Aguirre-Gutiérrez, J., E. Berenguer, I. O. Menor, et al. 2022. "Functional Susceptibility of Tropical Forests to Climate Change." *Nature Ecology & Evolution* 6: 878–889.

Argles, A. P., J. R. Moore, and P. M. Cox. 2022. "Dynamic Global Vegetation Models: Searching for the Balance Between Demographic Process Representation and Computational Tractability." *PLOS Climate* 1: e0000068.

Baker, C. A., L. Garcia-Carreras, W. Buermann, et al. 2021. "Robust Amazon Precipitation Projections in Climate Models That Capture Realistic Land–Atmosphere Interactions." *Environmental Research Letters* 16: 074002.

Bathiany, S., B. van der Bolt, M. S. Williamson, et al. 2016. "Statistical Indicators of Arctic Sea-Ice Stability—Prospects and Limitations." *Cryosphere* 10: 1631–1645.

Bauman, D., C. Fortunel, G. Delhaye, et al. 2022. "Tropical Tree Mortality Has Increased With Rising Atmospheric Water Stress." *Nature Climate Change* 608: 528–533.

Bochow, N., and N. Boers. 2023. "The South American Monsoon Approaches a Critical Transition in Response to Deforestation." *Science Advances* 9: eadd9973.

Boers, N. 2021. "Observation-Based Early-Warning Signals for a Collapse of the Atlantic Meridional Overturning Circulation." *Nature Climate Change* 11: 680–688.

Boers, N., M. Ghil, and T. Stocker. 2022. "Theoretical and Paleoclimatic Evidence for Abrupt Transitions in the Earth System." *Environmental Research Letters* 17: 093006.

Boettner, C., and N. Boers. 2022. "Critical Slowing Down in Dynamical Systems Driven by Nonstationary Correlated Noise." *Physical Review Research* 4: 013230.

Bohrnstedt, G. W., and A. S. Goldberger. 1969. "On the Exact Covariance Products of Random Variables." *Journal of the American Statistical Association* 64: 1439–1442.

Borchert, R. 1994. "Water Status and Development of Tropical Trees During Seasonal Drought." *Trees* 8: 115–125.

Boulton, C. A., P. Good, and T. M. Lenton. 2013. "Early Warning Signals of Simulated Amazon Rainforest Dieback." *Theoretical Ecology* 6: 373–384.

Boulton, C. A., T. M. Lenton, and N. Boers. 2022. "Pronounced Loss of Amazon Rainforest Resilience Since the Early 2000s." *Nature Climate Change* 12: 271–278.

Boysen, L. R., V. Brovkin, J. Pongratz, et al. 2020. "Global Climate Response to Idealized Deforestation in cmip6 Models." *Biogeosciences* 17: 5615–5638.

Cailleret, M., V. Dakos, S. Jansen, et al. 2019. "Early-Warning Signals of Individual Tree Mortality Based on Annual Radial Growth." *Frontiers in Plant Science* 9: 1964.

Camarero, J. J., A. Gazol, G. Sangüesa-Barreda, J. Oliva, and S. M. Vicente-Serrano. 2015. "To Die or Not to Die: Early Warnings of Tree Dieback in Response to a Severe Drought." *Journal of Ecology* 103: 44–57.

Ciemer, C., N. Boers, M. Hirota, et al. 2019. "Higher Resilience to Climatic Disturbances in Tropical Vegetation Exposed to More Variable Rainfall." *Nature Geoscience* 12: 174–179.

Cole, L. E. S., S. A. Bhagwat, and K. J. Willis. 2014. "Recovery and Resilience of Tropical Forests After Disturbance." *Nature Communications* 5: 3906.

Cowling, S. A., and Y. Shin. 2006. "Simulated Ecosystem Threshold Responses to Co-Varying Temperature, Precipitation and Atmospheric CO_2 Within a Region of Amazonia." *Global Ecology and Biogeography* 15: 553–556.

Cox, P. M., R. Betts, M. Collins, P. P. Harris, C. Huntingford, and C. Jones. 2004. "Amazonian Forest Dieback Under Climate-Carbon Cycle Projections for the 21st Century." *Theoretical and Applied Climatology* 78: 137–156.

Dias, D., and R. Marenco. 2016. "Tree Growth, Wood and Bark Water Content of 28 Amazonian Tree Species in Response to Variations in Rainfall and Wood Density." *iForest* 9: 445–451.

Drüke, M., B. Sakschewski, W. von Bloh, M. Billing, W. Lucht, and K. Thonicke. 2023. "Fire May Prevent Future Amazon Forest

Recovery After Large-Scale Deforestation." *Communications Earth & Environment* 4: 248.

Elsherif, A., R. Gaulton, and J. Mills. 2018. "Estimation of Vegetation Water Content at Leaf and Canopy Level Using Dual-Wavelength Commercial Terrestrial Laser Scanners." *Interface Focus* 8: 20170041.

Eltahir, E. A. B., and R. L. Bras. 1996. "Precipitation Recycling." *Reviews of Geophysics* 34: 367–378.

Forkel, M., L. Schmidt, R.-M. Zotta, W. Dorigo, and M. Yebra. 2023. "Estimating Leaf Moisture Content at Global Scale From Passive Microwave Satellite Observations of Vegetation Optical Depth." *Hydrology and Earth System Sciences* 27: 39–68.

Forzieri, G., V. Dakos, N. G. McDowell, A. Ramdane, and A. Cescatti. 2022. "Emerging Signals of Declining Forest Resilience Under Climate Change." *Nature* 608: 534–539.

Friend, A. D., W. Lucht, T. T. Rademacher, et al. 2014. "Carbon Residence Time Dominates Uncertainty in Terrestrial Vegetation Responses to Future Climate and Atmospheric CO_2." *Proceedings of the National Academy of Sciences* 111: 3280–3285.

Held, H., and T. Kleinen. 2004. "Detection of Climate System Bifurcations by Degenerate Fingerprinting." *Geophysical Research Letters* 31: L23207.

Hishe, H., L. Oosterlynck, K. Giday, W. de Keersmaecker, S. Somers, and B. Muys. 2021. "A Combination of Climate, Tree Diversity and Local Human Disturbance Determine the Stability of Dry Afromontane Forests." *Forest Ecosystems* 8: 1–16.

Kleinen, T., H. Held, and G. Petschel-Held. 2003. "The Potential Role of Spectral Properties in Detecting Thresholds in the Earth System: Application to the Thermohaline Circulation." *Ocean Dynamics* 53: 53–63.

Lehnebach, R., R. Beyer, V. Letort, and P. Heuret. 2018. "The Pipe Model Theory Half a Century on: A Review." *Annals of Botany* 121: 773–795.

Lenton, T. M., H. Held, E. Kriegler, et al. 2008. "Tipping Elements in the Earth's Climate System." *Proceedings of the National Academy of Sciences* 105: 1786–1793.

Levine, N. M., K. Zhang, M. Longo, et al. 2016. "Ecosystem Heterogeneity Determines the Ecological Resilience of the Amazon to Climate Change." *Proceedings of the National Academy of Sciences* 113: 793–797.

Liu, Y., M. Kumar, G. G. Katul, and A. Porporato. 2019. "Reduced Resilience as an Early Warning Signal of Forest Mortality." *Nature Climate Change* 9: 880–885.

Lovejoy, T. E., and C. Nobre. 2019. "Amazon Tipping Point: Last Chance for Action." *Science Advances* 5: eaba2949.

Luo, Y., Z. Shi, X. Lu, et al. 2017. "Transient Dynamics of Terrestrial Carbon Storage: Mathematical Foundation and Its Applications." *Biogeosciences* 14: 145–161.

Malhi, Y., L. E. Aragão, D. Galbraith, et al. 2009. "Exploring the Likelihood and Mechanism of a Climate-Change-Induced Dieback of the Amazon Rainforest." *Proceedings of the National Academy of Sciences* 106: 20610–20615.

McDowell, N., C. Allen, K. Anderson-Teixeira, et al. 2018. "Drivers and Mechanisms of Tree Mortality Inmoist Tropical Forests." *New Phytologist* 219: 851–869.

Morr, A., and N. Boers. 2024. "Detection of Approaching Critical Transitions in Natural Systems Driven by Red Noise." *Physical Review X* 14: 021037.

Nian, D., S. Bathiany, B. Sakschewski, et al. 2024. "Rainfall Seasonality Dominates Critical Precipitation Threshold for the Amazon Forest in the Lpjml Vegetation Model." *Science of the Total Environment* 947: 174378.

Nobre, C. A., and L. D. S. Borma. 2009. "'Tipping Points' for the Amazon Forest." *Current Opinion in Environmental Sustainability* 1: 28–36.

Oliveira, B. F., F. C. Moore, and X. Dong. 2022. "Biodiversity Mediates Ecosystem Sensitivity to Climate Variability." *Communications Biology* 5: 628.

Parry, I. M., P. D. Ritchie, and P. M. Cox. 2022. "Evidence of Localised Amazon Rainforest Dieback in CMIP6 Models." *Earth System Dynamics* 13: 1667–1675.

Poorter, L., F. Bongers, T. Aide, et al. 2016. "Biomass Resilience of Neotropical Secondary Forests." *Nature* 530: 211–214.

Poulter, B., F. Hattermann, E. Hawkins, et al. 2010. "Robust Dynamics of Amazon Dieback to Climate Change With Perturbed Ecosystem Model Parameters." *Global Change Biology* 16: 2476–2495.

Rogers, B. M., K. Solvik, E. H. Hogg, et al. 2018. "Detecting Early Warning Signals of Tree Mortality in Boreal North America Using Multiscale Satellite Data." *Global Change Biology* 24: 2284–2304.

Sakschewski, B., W. von Bloh, M. Drüke, et al. 2016. "Variable Tree Rooting Strategies Are Key for Modelling the Distribution, Productivity and Evapotranspiration of Tropical Evergreen Forests." *Biogeosciences* 18: 4091–4116.

Sakschewski, B., W. von Bloh, M. Drüke, et al. 2021. "Variable Tree Rooting Strategies Are Key for Modelling the Distribution, Productivity and Evapotranspiration of Tropical Evergreen Forests." *Biogeosciences* 18: 4091–4116.

Schaphoff, S., M. Forkel, C. Müller, et al. 2018. "Lpjml4—A Dynamic Global Vegetation Model With Managed Land—Part 2: Model Evaluation." *Geoscientific Model Development* 11: 1377–1403.

Schaphoff, S., W. von Bloh, A. Rammig, et al. 2018. "Lpjml4—A Dynamic Global Vegetation Model With Managed Land—Part 1: Model Description." *Geoscientific Model Development* 11: 1343–1375.

Scheffer, M., J. Bascompte, W. A. Brock, et al. 2009. "Early-Warning Signals for Critical Transitions." *Nature* 461: 53–59.

Scheffer, M., S. Carpenter, J. A. Foley, C. Folke, and B. Walker. 2001. "Catastrophic Shifts in Ecosystems." *Nature* 413: 591–596.

Schippers, P., M. Vlam, P. A. Zuidema, and F. Sterck. 2015. "Sapwood Allocation in Tropical Trees: A Test of Hypotheses." *Functional Plant Biology* 42: 697–709.

Shinozaki, K., K. Yoda, K. Hozumi, and T. Kira. 1964a. "A Quantitative Analysis of Plant Form-The Pipe Model Theory: II. Further Evidence of the Theory and Its Application in Forest Ecology." *Japanese Journal of Ecology* 14: 97–105.

Shinozaki, K., K. Yoda, K. Hozumi, and T. Kira. 1964b. "A Quantitative Analysis of Plant Form-The Pipe Model Theory: I. Basic Analyses." *Japanese Journal of Ecology* 14: 133–139.

Sitch, S., B. Smith, I. C. Prentice, et al. 2003. "Evaluation of Ecosystem Dynamics, Plant Geography and Terrestrial Carbon Cycling in the Lpj Dynamic Global Vegetation Model." *Global Change Biology* 9: 161–185.

Smith, T., and N. Boers. 2023a. "Global Vegetation Resilience Linked to Water Availability and Variability." *Nature Communications* 14: 498.

Smith, T., and N. Boers. 2023b. "Reliability of Vegetation Resilience Estimates Depends on Biomass Density." *Nature Ecology & Evolution* 7: 1799–1808.

Smith, T., D. Traxl, and N. Boers. 2022. "Empirical Evidence for Recent Global Shifts in Vegetation Resilience." *Nature Climate Change* 12: 477–484.

Smith, T., R.-M. Zotta, C. A. Boulton, T. M. Lenton, W. Dorigo, and N. Boers. 2023. "Reliability of Resilience Estimation Based on Multi-Instrument Time Series." *Earth System Dynamics* 14: 173–183.

Sohel, M., J. Herbohn, Y. Zhao, and J. McDonnell. 2023. "Sap Flux and Stable Isotopes of Water Show Contrasting Tree Water Uptake Strategies in Two Co-Occurring Tropical Rainforest Tree Species." *Ecohydrology* 16: e2589.

Song, X., X.-D. Zeng, and F. Li. 2016. "Evaluation of the Individual Allocation Scheme and Its Impacts in a Dynamic Global Vegetation Model." *Atmospheric and Oceanic Science Letters* 9: 38–44.

van Passel, J., P. Bernardino, S. Lhermitte, et al. 2024. "Critical Slowing Down of the Amazon Forest After Increased Drought Occurrence." *Proceedings of the National Academy of Sciences* 121: e2316924121.

Verbesselt, J., N. Umlauf, M. Hirota, et al. 2016. "Remotely Sensed Resilience of Tropical Forests." *Nature Climate Change* 6: 1028–1031.

Wagner, T. J. W., and I. Eisenman. 2015. "False Alarms: How Early Warning Signals Falsely Predict Abrupt Sea Ice Loss." *Geophysical Research Letters* 42: 10333–10341.

White, A., M. G. Cannell, and A. D. Friend. 1999. "Climate Change Impacts on Ecosystems and the Terrestrial Carbon Sink: A New Assessment." *Global Environmental Change* 9: S21–S30.

Wissel, C. 1984. "A Universal Law of the Characteristic Return Time Near Thresholds." *Oecologia* 65: 101–107.

Wu, D., G. G. Vargas, J. S. Powers, et al. 2022. "Reduced Ecosystem Resilience Quantifies Fine-Scale Heterogeneity in Tropical Forest Mortality Responses to Drought." *Global Change Biology* 28: 2081–2094.

Wu, M., S. Manzoni, G. Vico, A. Bastos, F. de Vries, and G. Messori. 2022. "Drought Legacy in Sub-Seasonal Vegetation State and Sensitivity to Climate Over the Northern Hemisphere." *Geophysical Research Letters* 49: e2022GL098700.

Zemp, D. C., C.-F. Schleussner, H. M. J. Barbosa, et al. 2017. "Self-Amplified Amazon Forest Loss due to Vegetation-Atmosphere Feedbacks." *Nature Communications* 8: 14681.

Supporting Information

Additional supporting information can be found online in the Supporting Information section.